Crystal Structure Analysis of Recombinant Rat Kidney Long Chain Hydroxy Acid Oxidase[†,‡]

Louise M. Cunane,[§] John D. Barton,[§] Zhi-wei Chen,[§] K. H. Diêp Lê,[||] David Amar,[||] Florence Lederer,[||] and F. Scott Mathews*[,§]

Department of Biochemistry and Molecular Biophysics, Washington University School of Medicine, St. Louis, Missouri 63110, and Laboratoire d'Enzymologie et Biochimie Structurales, UPR 9063, Centre National de la Recherche Scientifique, 91198 Gif-sur-Yvette Cedex, France

Received June 30, 2004; Revised Manuscript Received November 12, 2004

ABSTRACT: Long chain hydroxy acid oxidase (LCHAO) is a member of an FMN-dependent enzyme family that oxidizes L-2-hydroxy acids to ketoacids. LCHAO is a peroxisomal enzyme, and the identity of its physiological substrate is unclear. Mandelate is the most efficient substrate known and is commonly used in the test tube. LCHAO differs from most family members in that one of the otherwise invariant active site residues is a phenylalanine (Phe23) instead of a tyrosine. We now report the crystal structure of LCHAO. It shows the same $\beta_8\alpha_8$ TIM barrel structure as other structurally characterized family members, e.g., spinach glycolate oxidase (GOX) and the electron transferases yeast flavocytochrome b_2 (FCB2) and *Pseudomonas putida* mandelate dehydrogenase (MDH). Loop 4, which is mobile in other family members, is visible in part. An acetate ion is present in the active site. The flavin interacts with the protein in the same way as in the electron transferases, and not as in GOX, an unexpected observation. An interpretation is proposed to explain this difference between GOX on one hand and FCB2 and LCHAO on the other hand, which had been proposed to arise from the differences between family members in their reactivity with oxygen. A comparison of models of the substrate bound to various published structures suggests that the very different reactivity with mandelate of LCHAO, GOX, FCB2, and MDH cannot be rationalized by a hydride transfer mechanism.

Long chain L-2-hydroxy acid oxidase (LCHAO)[1] is a tetrameric peroxisomal enzyme (EC 1.1.3.15, isozyme B). It belongs to an evolutionary family of FMN-dependent enzymes which have as substrates diverse L-2-hydroxy acids. It is known as an isozyme of glycolate oxidase (GOX, EC 1.1.3.15, isozyme A), one of the best characterized family members. Other well-studied relatives are yeast flavocytochrome b_2 or L-lactate dehydrogenase (FCB2) (*1*), mycobacterial lactate monooxygenase (LMO) (*2*), and, more recently, lactate oxidase from *Aerococcus viridans* (LOX) (*3*) and mandelate dehydrogenase from *Pseudomonas putida* (MDH) (*4*). These enzymes present unmistakable sequence similarity [45% identity between rat HAO and spinach GOX (*5*)]. Thus far, three crystal structures of family members have been determined: those of GOX (*6*, *7*), FCB2 (*8*), and MDH−GOX2, a soluble chimeric mutant form of MDH (*9*, *10*). A comparison between these three structures indicates very similar three-dimensional configurations with an identical $\beta_8\alpha_8$ barrel fold, and identical active site residues (*11*). Furthermore, these molecules form tetrameric oligomers possessing circular 4-fold symmetry in which the interactions between monomers are also well conserved. These results suggest an identical chemical mechanism for substrate dehydrogenation (the flavin reductive half-reaction).

On the other hand, the flavin oxidative half-reaction differs among the family members. GOX and LCHAO, as dehydrogenase-oxidases, are reoxidized by dioxygen in a two-electron reaction; FCB2, as a dehydrogenase-electron transferase, requires a monoelectronic acceptor, in this case heme b_2 located in the same molecular edifice. MDH, also a dehydrogenase-electron transferase, requires small lipophilic organic molecules such as ubiquinone that reside in the cytoplasmic membrane as the monoelectronic acceptor. GOX reacts rapidly with molecular oxygen, while both FCB2 and MDH react slowly with it.

LCHAO from rat kidney and liver was first described as an L-amino acid oxidase (*12*) and then found to be more active with L-2-hydroxy acids (*13*). Its cDNA was cloned from rat kidney (*14*). This led to the identification of two

[†] This work was supported by NIH Grant GM-20530 and NSF Grant MCB-0091084 (F.S.M.) and by the CNRS (F.L.).

[‡] Crystallographic coordinates have been deposited in the Protein Data Bank as entry 1tb3.

* To whom correspondence should be addressed: Department of Biochemistry and Molecular Biophysics, Washington University School of Medicine, St. Louis, MO 63110. E-mail: mathews@biochem.wustl.edu. Phone: (314) 362-1080. Fax: (314) 362-7183.

[§] Washington University School of Medicine.

[||] Centre National de la Recherche Scientifique.

[1] Abbreviations: EG, ethylene glycol; FDH, flavodehydrogenase; FCB2, flavocytochrome b_2 from *Saccharomyces cerevisiae*; GOX, spinach glycolate oxidase; LCHAO, rat long chain hydroxy acid oxidase; MDH, mandelate dehydrogenase from *Pseudomonas putida*; MDH−GOX2, soluble mandelate dehydrogenase chimera in which the 39-residue membrane-binding segment of MDH is replaced with the corresponding 20-residue segment of glycolate oxidase; NCS, noncrystallographic symmetry; rmsd, root-mean-square deviation; TACA, 4-carboxy-5-(1-pentyl)hexylsulfanyl-1,2,3-triazole; TKP, 3-decyl-2,5-dioxo-4-hydroxy-3-pyrroline; WT, wild type.

10.1021/bi048616e CCC: $30.25
Published on Web 01/14/2005

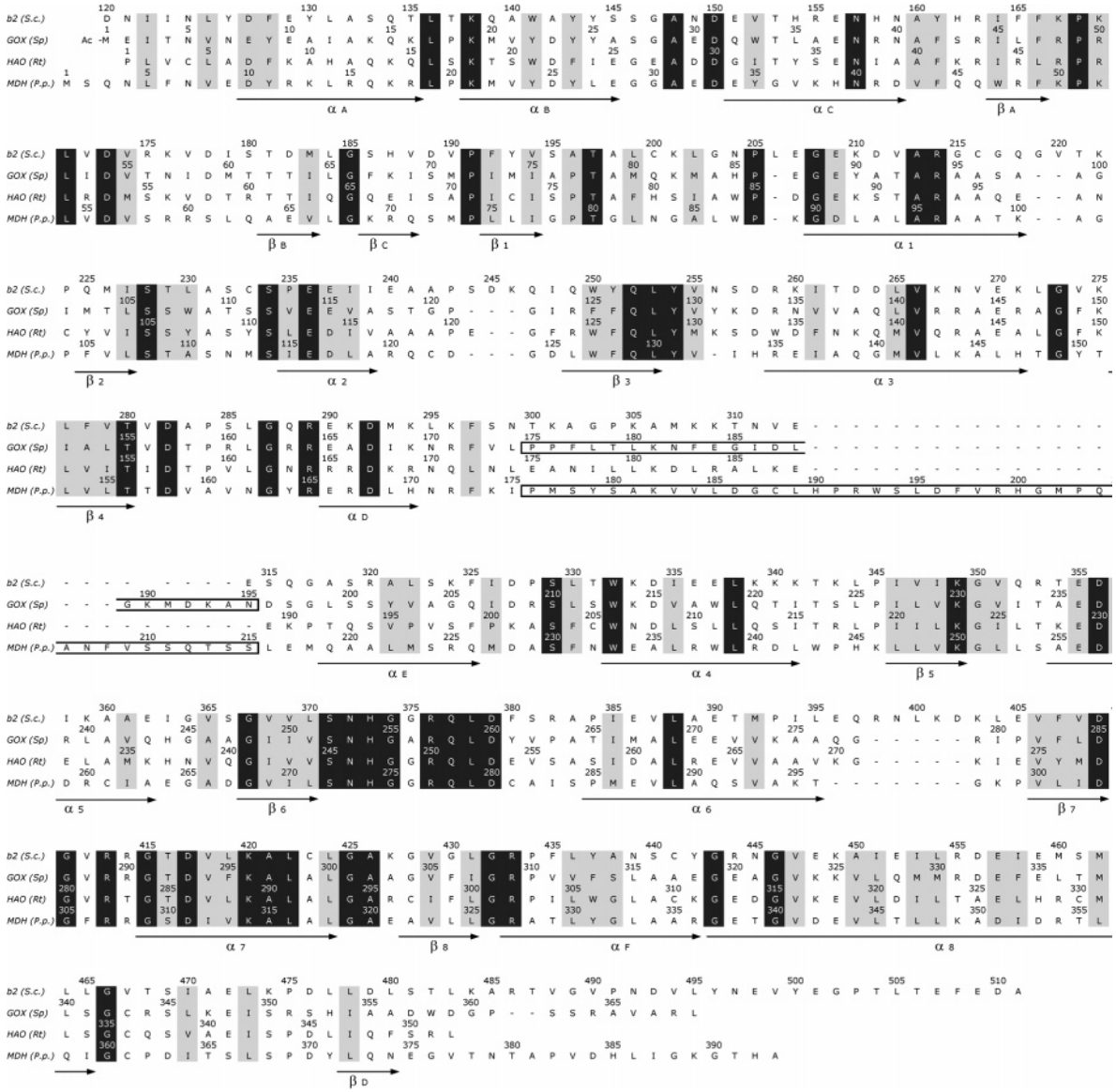

FIGURE 1: Sequence alignment: *b2 (S.c.)*, flavocytochrome b_2 from *S. cerevisiae*; *GOX (Sp)*, spinach glycolate oxidase; *HAO (Rt)*, rat long chain hydroxy acid oxidase; *MDH (P.p.)*, mandelate dehydrogenase from *P. putida*. The black background denotes residues invariant in the four sequences, and the gray background denotes conservative substitutions. The framed segments correspond to the GOX sequence that was engineered into the MDH sequence and the replaced MDH sequence. The alignment is adapted from that presented in ref *11*, which is based on the comparison between the FCB2 and GOX crystal structures. The arrows below the sequences indicate the position of secondary structure elements in GOX.

mRNAs differing by a 9 bp insertion within the coding sequence, resulting in a three-amino acid residue insertion in the protein; the shorter form (isozyme β1) appears to represent ~90% of the protein expressed in rat kidney (*15*). The isoforms can now be separately expressed in *Escherichia coli*.

It appeared to be of interest to obtain structural data concerning LCHAO, for several reasons. First, the enzymes in the family differ in the length and sequence of what is now known as the barrel loop 4, situated between β-strand 4 and α-helix 4 of the TIM barrel (Figure 1). In all but one of the known structures, part of loop 4 is disordered: residues 300−316 in the FCB2 crystal structure first reported (*8*) [with some variation among different crystal forms reported later (*16*, *17*)] and residues 189−198 for GOX; in the 1.35 Å resolution structure of MDH−GOX2, GOX-derived loop 4 is entirely defined (*10*). The visible stretch of loop 4 adopts in part a different conformation between the FCB2 and GOX structures, but in both cases, the borders of the invisible region lie between 15 and 25 Å away from the FMN. The three-residue insertion mentioned above in LCHAO isozyme β2 (between positions 188 and 189 of isozyme β1) is located at the edge of the equivalent GOX disordered region. Surprising is the fact that this insertion appears to be responsible for the spectrally analyzed pK_a differences in the flavin N3−H ionization: pH 7.9 for isozyme β1 and pH 7.5 for isozyme β2 (*15*). In view of the distance in the GOX structure between the corresponding region and flavin N3, it appeared to be surprising that the insertion could have such a long-distance influence, especially if it is mobile; these results suggested that loop 4 had a different conformation in LCHAO and/or that it could close in on the FMN upon substrate binding. Indeed, a more recently determined structure of glycolate oxidase in complex with several inhibitors indicated the possibility of conformational changes in loop 4 (*18*).

A second reason for determining the LCHAO crystal structure is the enzyme specificity, or lack thereof. Whereas both FCB2 and GOX have a marked specificity for their physiological substrates, L-lactate and glycolate, respectively, the LCHAO physiological substrate is not known. In rigorous kinetic terms, as judged from k_{cat}/K_m values, LCHAO has been found to be most efficient with L-mandelate, somewhat less so with L-2-hydroxyisocaproate, L-phenyllactate, and DL-2-hydroxy-4-methylthiobutanoate; its efficiency decreases drastically together with the substrate chain length (*15*). However, over the years, LCHAO was also proposed to act on adducts between glyoxylate and sulfhydryl compounds (*19*, *20*), to be capable of oxidizing thyroxin and triiodothyronin (*21*), and to contribute to the metabolism of some nephrotoxic cysteine conjugates such as 1,2-dichlorovinylcysteine (*22*, *23*). Even more recently, the production of methylguanidine (a metabolite involved in a variety of uremic syndromes) from creatol was ascribed to LCHAO (*24*, *25*). Noticeably, creatol [hydroxycreatinine, or 2-amino-5-hydroxy-1-methyl-4(5*H*)-imidazolone] is not a 2-hydroxy carboxylic acid.

A physiological function in fatty acid α-oxidation was suggested for three human homologues of LCHAO, the genes of which were recently cloned and expressed (*26*). HAOX1 is most similar to GOX, while the sequences of HAOX2 and HAOX3 are 74.0 and 82.6% identical to the rat LCHAO sequence. HAOX3 was subsequently found to be a mouse protein (*27*). HAOX1 had specificity for glycolate, whereas HAOX3 was more active with 2-hydroxy octanoate. Most noticeably, rat LCHAO, human HAOX2, and mouse HAOX3 share a Tyr to Phe substitution of an active site residue implicated in substrate binding [position 143 of FCB2, position 24 of GOX, position 23 of LCHAO, and position 26 of MDH (Figure 1)].

In this paper, we describe the crystal structure of rat kidney LCHAO isozyme β1, as well as kinetic experiments designed to test the enzyme activity toward long chain α-hydroxy acids. Although the enzyme extracted initially from rat kidney was crystallized in ammonium sulfate (*21*), crystals of the recombinant isozyme obtained by the same method were unsuitable for structure determination, and we were forced to devise a different crystallization procedure. This work was presented earlier in preliminary form (*28*).

EXPERIMENTAL PROCEDURES

Crystallization and Data Collection. LCHAO was prepared as described previously (*15*). Crystals of LCHAO were grown by the sitting drop vapor diffusion method (*29*). Five microliters of a protein solution [at 10 mg/mL in 0.1 M Tris buffer (pH 7.5)] was mixed with 5 μL of a reservoir solution [0.4 M sodium acetate and 0.2 M sodium citrate (pH 6.5)] and allowed to equilibrate at 4 °C. X-ray data were collected to 2.3 Å resolution from a crystal [soaked for 5 min in 0.4 M sodium acetate, 0.2 M sodium citrate (pH 6.5), and 25% glycerol] at ~100 K on beamline 19ID at the Structural Biology Center of the Advanced Photon Source (Argonne National Laboratories, Argonne, IL). The crystal was primitive orthorhombic with the following unit cell parameters: $a = 114.82$ Å, $b = 150.97$ Å, and $c = 222.37$ Å. It contained two homotetramers of 156 kDa each in the asymmetric unit. The data were processed with HKL2000 (*30*), resulting in an R_{merge} of 5.0%. Systematic absences of axial reflections $h00$, $0k0$, and $00l$ when h, k, and l are odd indicated that the space group symmetry was $P2_12_12_1$. The data collection statistics are summarized in Table 1.

Table 1: Data Collection and Refinement Statistics

Crystallographic Data	
space group	$P2_12_12_1$
unit cell parameters	$a = 114.82$ Å, $b = 150.97$ Å, $c = 222.37$ Å
resolution range (Å)	40−2.30
no. of observed reflections[a]	600025
no. of unique reflections[a]	159633
completeness (%)	93.0 (79.4)[b]
redundancy (%)	3.9 (2.7)[b]
average $I/\sigma(I)$[c]	20.6 (3.4)[b]
R_{merge}[d] (%)	5.0 (28.6)[b]
Refinement Statistics	
no. of reflections in the working set[e,f]	135564
no. of reflections in the test set[e,f]	7147
R_{work}[g] (%)	23.9
R_{free}[g] (%)	26.9
no. of protein non-H atoms	20448
no. of polypeptide chains	8
no. of FMN atoms	248
no. of acetate atoms	32
no. of water molecules	900
average B-factor (Å^2)	
chain A	36.5
chain B	42.8
chain C	41.1
chain D	39.9
chain E	43.9
chain F	33.5
chain G	40.0
chain H	39.2
solvent	32.5
rms deviations	
bond lengths (Å)	0.007
bond angles (deg)	1.27
rms ΔB (m/m, Å^2)[h]	3.1
rms ΔB (m/s, Å^2)[h]	3.9
rms ΔB (s/s, Å^2)[h]	5.1

[a] Observed reflections with intensities $I < -3\sigma(I)$ were rejected during data processing. [b] Values in parentheses are for the last shell (2.34−2.30 Å). [c] $I/\sigma(I)$ is the signal-to-noise ratio for merged reflections. [d] $R_{merge} = \sum_h\sum_i I(h) - I_i(h)/\sum_h\sum_i I_i(h)$, where $I_i(h)$ and $I(h)$ are the ith and mean measurements of reflection h, respectively. [e] During refinement, structure factors with a magnitude of less that zero were rejected. [f] The test set and working set of reflections are set aside for cross validation (*36*) during refinement. [g] $R = \sum_h|F_o - F_c|/\sum_h|F_o|$, where F_o and F_c are the observed and calculated structure factor amplitudes of reflection h, respectively. R_{free} is the R value for the test reflection data set, and R_{work} is the R value for the working reflection data set. [h] Root-mean-square difference in B-factor for bonded atoms; m/m, m/s, and s/s represent main chain−main chain, main chain−side chain, and side chain−side chain bonds, respectively.

Upon examination of the X-ray data intensities, it was noted that all reflections with l odd were weak compared with those with l even. The mean ratio of structure factor amplitudes for odd to even l values was approximately 0.25, suggestive of the presence of a superlattice. Verification of the space group symmetry and identification of the subunit arrangement within the asymmetric unit are described in the Supporting Information.

Structure Determination and Refinement. The structure of LCHAO was determined by molecular replacement analysis with AMORE (*31*) using a homotetramer of glycolate oxidase [GOX, PDB entry 1GOX (*32*)] as a search model.

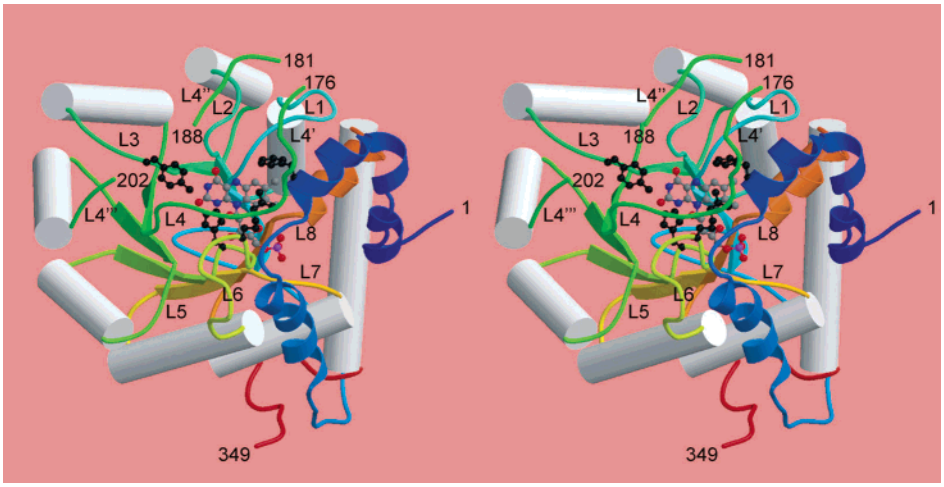

FIGURE 2: Ribbon diagram of LCHAO. The eight α-helices of the TIM barrel motif are shown as gray cylinders, while the remainder of the structure is a ribbon colored blue near the N-terminus, progressing through green, yellow, and orange to red near the C-terminus. For clarity, minor strands and helices are shown as coils except for helices α_A, α_B, and α_C near the N-terminus and helix α_F near the C-terminus (Figure 1). The eight loops between β-strands and α-helices of the $\beta_8\alpha_8$ motif are labeled L1−L8 with the longest loop, L4, labeled in four places (L4, L4′, L4″, and L4‴). The visible ends of the disordered segments in L4, residues 176, 181, 188, and 202, are labeled as are the N- and C-termini. The FMN in the center is shown as a ball and stick in atom colors (gray for carbon, blue for nitrogen, and red for oxygen), and active site residues Phe23, Arg250, His247, and Tyr129 are colored black, starting at the top right and moving clockwise to the top left, and surround the active site pocket above the flavin ring. This figure was prepared using MOLSCRIPT (*61*) and rendered with RASTER3D (*62*).

The GOX search model was stripped of FMN, and all nonidentical side chains between the two proteins (∼54%) were replaced with alanine. A clear-cut solution with two independent tetramers in the asymmetric unit was obtained.

The amino acid sequence of LCHAO (*5*, *14*) was fit to the resulting map. Initially, residues 172−201 were found to be missing in all eight subunits. Structure refinement was carried out using X-Plor (*33*) and later CNS (*34*). The outer resolution limit was gradually extended until all data from 40 to 2.3 Å were refined, using a correction for bulk solvent. Tight NCS restraints, with a weight of 300, were initially applied to all residues of the eight monomers of the asymmetric unit and subsequently were reduced to 50; two short segments involved in close intersubunit contact (residues 132−136 and 210−218) were then released from NCS restraints. The FMN cofactor and a small molecule ligand (tentatively identified as acetate) were placed into the active sites of the eight subunits, and water molecules were gradually introduced into the model. At this point, weak, continuous density for residues 172−176 was identified, and these residues were introduced into all eight subunits and refined using NCS restraints for this segment. An additional segment of weak electron density, visible on the molecular surface, was then modeled by residues 181−188 in four of the eight subunits and by shorter segments in the remaining subunits. These additional residues were included in the refinement, but were not restrained by NCS. Several more water molecules were then added, and R and R_{free} fell to final values of 0.239 and 0.269, respectively. The final refinement statistics are presented in Table 1.

Enzyme Kinetics. Assays were carried out in 0.1 M imidazolium/HCl buffer and 1 mM EDTA (pH 7.5) at 30 °C with a Uvikon 943 spectrophotometer. The hydroxy acids concentrations were varied at a constant 2,6-dichlorophenolindophenol concentration (70 μM). Results are the average of two independent experiments.

RESULTS

Quality of the Structure. Continuous electron density could be modeled in all eight subunits of LCHAO from Pro1 at the N-terminus to Phe349, except for a segment spanning residues 177−201, where only portions of the sequence could be modeled (see below); the last three residues of the mature sequence, Ser350, Arg351, and Leu352 [the peroxisomal targeting sequence (*35*)], are also absent from the electron density. The electron density within the partially ordered segment comprising residues 171−201 (which could not be visualized in early maps) is especially weak. There, the average temperature factor is 85 Å^2 compared to an average B of 38 Å^2 for the remainder of the protein. An analysis of the Ramachandran plot (*36*, *37*) of the refined structure indicates that 98.7% of the amino acids are in the most favored and additionally allowed regions of conformational space; 30 amino acids (1.3%) are in the generously allowed region, and one is in the disallowed region. These latter amino acids are contained within the sets of residues Asp29, Phe79, Asn173, Asp182, and Gln251, and their disfavored conformations are distributed among the eight subunits. Two of these (Asn173 and Asp182) are located within the segment of weak electron density and high temperature factor described above.

Overall Description of the Molecule. The eight subunits of LCHAO in the asymmetric unit form an octamer with 422 molecular point group symmetry. Each monomer contains the expected $\beta_8\alpha_8$ barrel structure (Figure 2) as well as one molecule of FMN. In addition, one acetate anion bound at the active site was identified on the basis of the shape of the electron density (Figure 3), its presence in the crystallization medium, and the electropositive environment. The asymmetric unit also contains 900 solvent molecules.

The 24-residue segment between residues Ala176 and Ala202 that is only partially ordered is located in loop 4 of the β-barrel and corresponds approximately to the disordered segments identified in the other α-hydroxy acid oxidizing

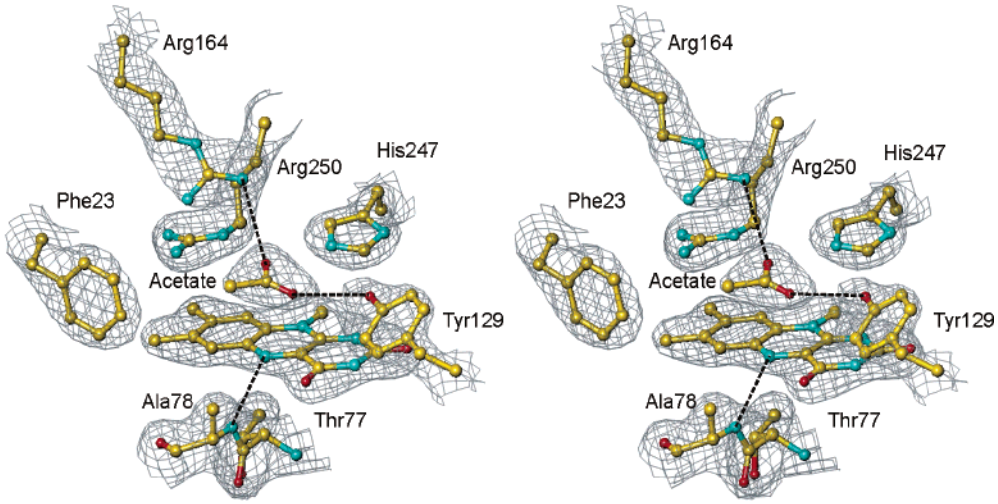

FIGURE 3: Electron density of LCHAO at the active site showing the acetate anion, flavin ring, five of the highly conserved surrounding side chains (Phe23, Tyr129, Arg164, His247, and Arg250), and the Thr77-Ala78 dipeptide of β-strand 1. The atoms are colored yellow for carbon, red for oxygen, and cyan for nitrogen. Hydrogen bonds between the carboxylate oxygens of acetate and the side chains of Arg164 and Tyr129 and between N5 of flavin and N of Ala78 are shown as dashed lines. The electron density map is contoured at the 1σ level. This figure was prepared using Turbo-Frodo (*63*).

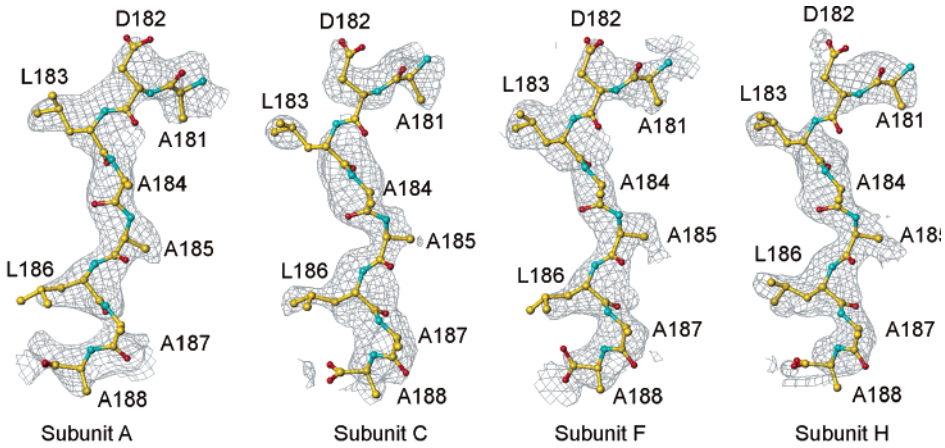

FIGURE 4: Electron density of LCHAO in subunits A, C, F, and H into which the ordered peptide segment of Ala181−Ala188 could be modeled. The atom coloring scheme is the same as in Figure 3. The electron density map is contoured at the 0.75σ level. This figure was prepared using Turbo-Frodo (*63*).

enzyme family members (Figure 1). In four of the subunits (A, C, F, and H), the Lys181−Glu188 segment could be modeled into the electron density (Figure 4); in three subunits (B, D, and G), only three to five residues of this segment (185−187, 183−187, and 184−188) could be fit, and in one subunit (E), none of them could.

The ordered octapeptide of LCHAO loop 4 is located at the top of the TIM barrel, above the flavin ring and the enzyme active site (Figure 2). Its amino-terminal end, at residue Ala181, is ~6 Å from the carboxyl terminus of Ala176 which would allow sufficient room for the missing intervening tetrapeptide to coil over the nearby protein surface. The carboxyl-terminal end of the octapeptide, at residue Ala188, is ~10 Å from the amino-terminal end of Ala202. Since the intervening peptide loop must accommodate 13 residues, it would be long enough to make contact with several residues within the mouth of the active site as well as elsewhere over the protein surface. Also, residue Ala188 is located approximately 13 Å from atom O4 of the flavin ring, the closest atom on FMN.

Active Site of LCHAO. The FMN is located at the C-terminal end of the β_8 barrel of the TIM barrel motif that is common to the α-hydroxy acid oxidizing family of enzymes (Figure 2). The *re* face of its flavin ring is in close contact with strand β1 of the barrel with its N5 atom, accepting a hydrogen bond from the peptide amide group of Ala78 (Figure 3). Other hydrogen bonding interactions of the flavin ring involve the side chains of Ser105 (with O4 of flavin), Gln127 (with N3 of flavin), Thr155 (with O2 of flavin), and Lys223 (with N1 of flavin and O2′ of the ribityl group). This mode of flavin binding is identical to that in FCB2 and MDH−GOX2, involving hydrogen bonding interactions with conserved residues, but different from that in GOX (see below).

The acetate anion is located above the flavin plane and parallel to it (Figure 3). The O1A atom of acetate (as inferred from its chemical surroundings) forms a hydrogen bond with $N^{\eta 2}$ of Arg164 (at an average distance of 3.17 Å), and the O1B atom forms one with O^{η} of Tyr129 (average distance of 3.18 Å); the methyl group is directed toward the phenyl ring of Phe23 more than 4 Å away. Surprisingly, the $N^{\delta 2}$ atom of His247 does not appear to form a hydrogen bond to either oxygen of acetate, although the position of the acetate ion in the eight subunits is somewhat variable, consistent

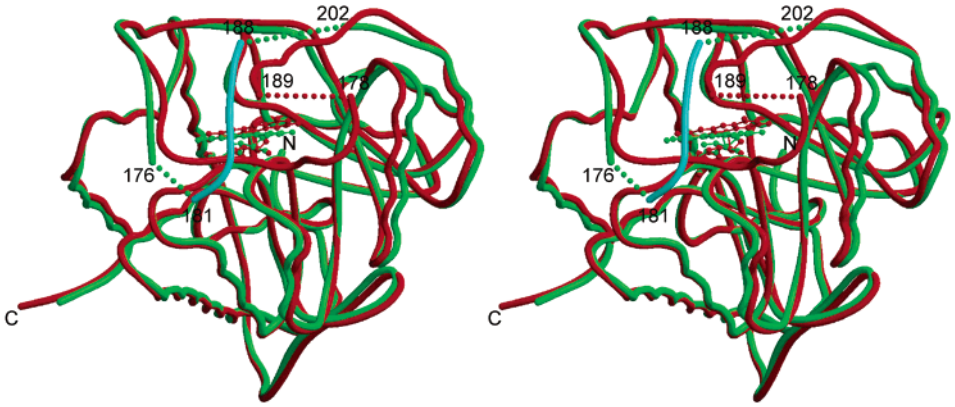

FIGURE 5: Comparison of the ribbon chain tracings of the isolated subunits of GOX (green) and LCHAO (red) except for the Ala181−Ala188 ordered peptide which is cyan. The disordered regions of both structures are indicated with dotted lines, and their end points are labeled. The relative displacements of the flavin rings in the two structures (LCHAO in red and GOX in green) can also be seen. This figure was prepared using MOLSCRIPT (*61*) and rendered with RASTER3D (*62*).

with its somewhat higher average *B* factor (∼50 Å^2 compared with values of 40 Å^2 for the average protein atom and 34 Å^2 for the average flavin ring atom).

Despite the apparent openness of the active site (Figure 2), the flavin ring is only slightly exposed to solvent. In the absence of the acetate ion, its solvent-exposed surface area is ∼11 Å^2 with the N5 atom exhibiting the greatest extent of exposure (5 Å^2). When acetate in included in the calculation, the accessible surface area of the flavin drops to nearly zero. Surprisingly, if the ordered octapeptide of loop 4 (residues 181−188) is omitted from the calculation, the accessible surface area of the flavin ring does not change, indicating that this portion of loop 4, at least, plays no role in blocking the active site of the enzyme.

Surrounding the active site of LCHAO, occupied by acetate in this instance, are seven residues that are highly conserved among the α-hydroxy acid oxidizing enzyme family members. These are Phe23, Tyr129, Asp157, Arg164, Lys223, His247, and Arg250. Of these, only Phe23 differs among them, being tyrosine in all other enzymes of known sequence except for human HAOX2 and mouse HAOX3. All of these side chains except Arg164 and, to a lesser extent, Phe23 are located in approximately the same position (to ∼0.5−1.0 Å) in both FCB2 and MDH−GOX2. In GOX, the side chain displacement is somewhat greater, probably because of an altered mode of flavin binding compared with that of the other family members (see below).

Structural Comparison with Glycolate Oxidase. When the individual subunits of LCHAO and GOX are aligned, the root-mean-square deviation (rmsd) is 0.90 Å for 320 equivalent Cα atoms with 48% sequence identity for matched atoms (Table 2). Interestingly, the second half of LCHAO matches that of GOX considerably more closely than the first half (Table 2). The structural similarity extends to the level of the full tetramers and to the octamers (Table 2). The interactions between the pairs of subunits, although similar structurally, are not well conserved chemically; 13 hydrogen bonds connect pairs of subunits in LCHAO and 19 in GOX, but only six are at conserved positions while three involve identical residues. Likewise, the buried surface area between subunits in the LCHAO tetramer is 1375 Å^2 per subunit compared to a value of 1500 Å^2 for GOX. These observations may indicate a less stable tetramer for LCHAO than for GOX, although lower oligomerization states of LCHAO were not observed in solution (*38*).

Table 2: Structural Comparisons between Various Oligomeric States of LCHAO and GOX

protein entity	rmsd (Å)	no. of residues compared	sequence identity (%)
monomer (full)	0.90	320	48
monomer (first half)[a]	1.03	174	42
monomer (second half)[a]	0.65	148	56
tetramer	0.99	1274	–
octamer	1.22	2539	–

[a] The first half of LCHAO consists of residues 1−174 and the second half of residues 202−349.

The most striking differences between LCHAO and GOX when their monomers are superimposed are the orientations of the flavin ring and the positions of the poorly ordered segments of loop 4. In GOX, the plane of the flavin ring is tilted by ∼15° from that in LCHAO (Figure 5) and the hydrogen bonding interactions of the flavin ring atoms with the protein are altered. The flavin N5 atom in GOX forms a hydrogen bond with a water molecule rather than with a peptide amide group of strand β1. O4 of GOX is hydrogen bonded to O$^{\eta}$ of Tyr129, while N3 appears not to form any hydrogen bond. However, the O2 and N1 atoms of flavin form hydrogen bonds to O$^{\gamma 1}$ of Thr155 and N$^{\zeta}$ of Lys230, residues equivalent to their hydrogen bonding partners in LCHAO. These side chains are somewhat displaced from their positions in LCHAO as are those of the seven highly conserved active site residues of the enzyme family described in the previous section.

A comparison of the disordered loop 4 segments in LCHAO and GOX is shown in Figure 5. In GOX, the disordered loop 4 segment of the TIM barrel is located between residues 188 and 198, while in LCHAO, it is between residues 176 and 202, with the intervening segment of residues 181−187 being ordered. It appears that the ordered portions of the variable gap segment of loop 4 of LCHAO and GOX differ significantly from each other. In LCHAO, the position of the ordered octapeptide of residues 181−187 may represent a "snapshot" of one of several possible conformations of this segment normally sampled by the LCHAO molecule.

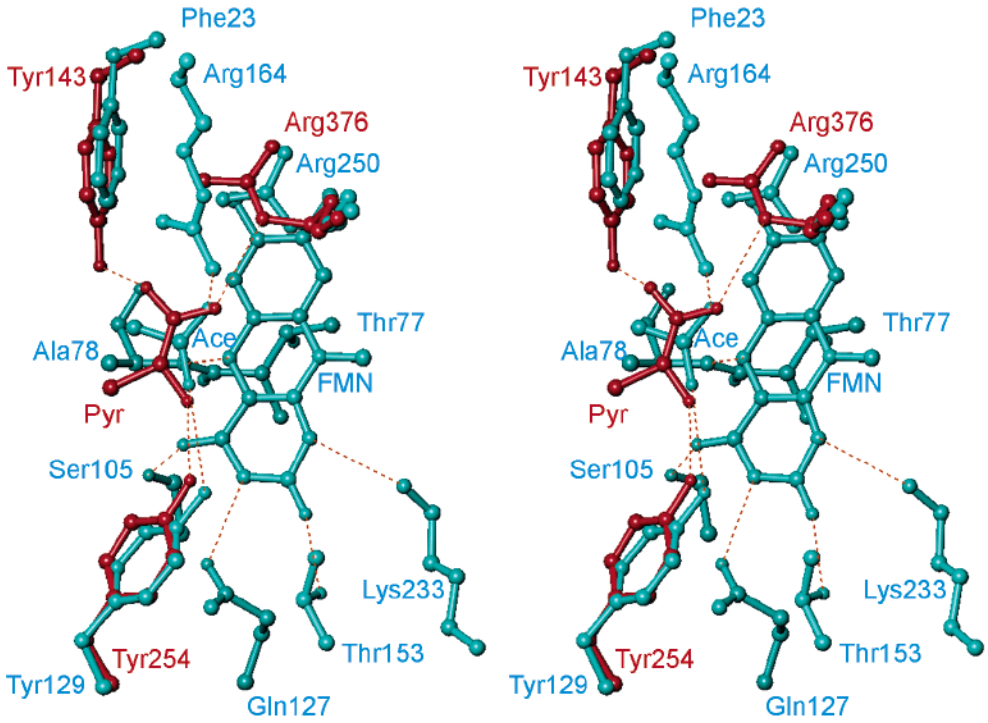

FIGURE 6: Active site of LCHAO (blue) showing the residues that interact with the flavin ring and the acetate anion ligand in the structure. Also shown is the pyruvate ligand of FCB2 superimposed on the LCHAO structure, three FCB2 side chains that interact with it (red), and the counterpart side chains in LCHAO (blue). This figure was prepared using Turbo-Frodo (*63*).

Table 3: Steady-State Kinetic Parameters for Some HAO Substrates

substrate	K_m (mM)	k_{cat} (s^{-1})	k_{cat}/K_m (mM^{-1} s^{-1})
L-mandelate[a]	0.11 ± 0.02	1.16 ± 0.13	10.5 ± 0.11
L-2-hydroxy octanoate	0.046 ± 0.005	0.99 ± 0.03	21.4 ± 0.17
L-2-hydroxy palmitate	1.36 ± 0.64	0.34 ± 0.09	0.25 ± 0.14
L-lactate[b]	6.1 ± 1.7	0.26 ± 0.02	0.04 ± 0.01

[a] From ref *59*. [b] From ref *14*.

Table 4: Comparison of Kinetic Parameters of GOX, LCHAO, FCB2, and MDH Using Mandelate as the Substrate

		LCHAO[b]			
parameter	GOX[a]	WT	F23Y	FCB2[c]	MDH−GOX2[d]
k_{cat} (s^{-1})	0.09	1.16	0.13	0.012	205
K_m (mM)	58	0.11	0.01	0.36	0.085
k_{cat}/K_m (M^{-1} s^{-1})	1.5	10.5×10^3	13×10^3	33	2412×10^3

[a] From ref *39*; temperature of 25 °C. [b] From ref *59*; temperature of 30 °C. [c] From ref *44*; temperature of 30 °C. [d] From ref *60*; temperature of 20 °C.

Further Probing of the LCHAO Specificity. The recently described human and mouse homologues that have an active site Phe instead of the otherwise invariant Tyr at position 23, HAOX2 and HAOX3, were found to be active with 2-hydroxy octanoate and 2-hydroxy palmitate, respectively (*26*). We tested these two longer chain hydroxy acids. The results are shown in Table 3. 2-Hydroxy octanoate is only 2-fold more efficient than mandelate, while 2-hydroxy palmitate is turned over with a definitely lower efficiency, although somewhat more efficiently than lactate. These results do not shed light on the actual physiological substrate for this peroxisomal enzyme.

DISCUSSION

LCHAO Specificity and Mechanistic Implications for the Reductive Half-Reaction. When the structures of various ligand complexes of FCB2 and GOX (*8*, *16*−*18*, *39*−*41*) are compared, the organic ligands seen in these structures take up a variety of orientations, but they all lie more or less in the same plane and at the same distance from the flavin, in keeping with observations on other flavoenzymes (*42*). Nevertheless, modeling studies suggest that, for this enzyme family, the only productive binding mode for a normal substrate is one in which the carboxylate is in hydrogen bonding and electrostatic interactions with one or both of the active site arginines and the closest tyrosine (Phe in LCHAO), as exemplified by the binding of pyruvate to FCB2 (*43*, *44*). In LCHAO, the acetate orientation is ~90° away from that of the pyruvate anion in FCB2 (Figure 6). However, since acetate is not a substrate of LCHAO and its presence is probably accidental, it provides little insight into the catalytic mechanism.

Mandelate is the physiological substrate for MDH and is the best substrate known for LCHAO; it also shows weak activity with FCB2 and GOX. Table 4 compares the kinetic values found in the literature for the four enzymes. Mandelate has a rather similar K_m value for the first three of these enzymes, but its turnover rate with MDH is 200-fold higher than with LCHAO and nearly 20000-fold higher than with FCB2. The low LCHAO mandelate activity relative to MDH cannot be due to the active site substitution of Phe for the otherwise invariant Tyr since the Phe23Tyr mutant of LCHAO has an even lower turnover rate than the WT (Table 3). With GOX, the situation is slightly different; while the low turnover rate with mandelate (~200-fold lower than for glycolate) is intermediate between those with FCB2 and LCHAO, its K_m value is very high. It is striking how much higher the catalytic efficiency of MDH for its physiological

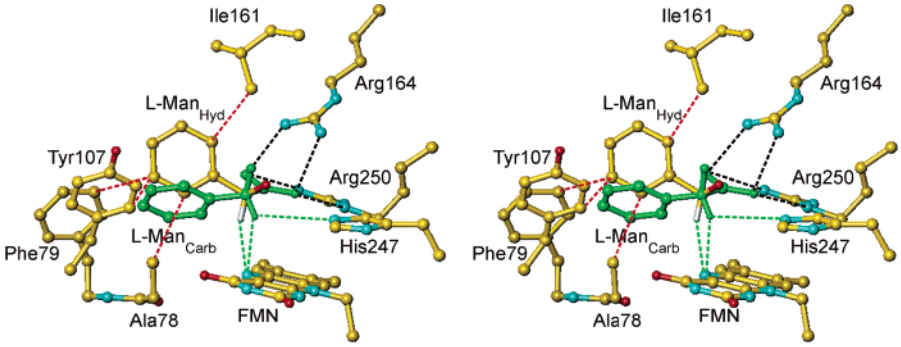

FIGURE 7: Models for the binding of L-mandelate into the active site of LCHAO, both in a configuration appropriate for a hydride transfer mechanism (L-Man$_{Hyd}$, atom colors as in Figure 3 with hydrogen in white) and for a carbanion mechanism (L-Man$_{Carb}$, green). Also shown are the active site atoms of LCHAO that interact with the hydride transfer model. The positions of the carboxylate and C2 atoms are the same for the two L-mandelate models. The black dashed lines represent hydrogen bonds between the guanidine atoms of Arg164 and Arg250 and the mandelate carboxylate oxygen atoms. Red dashed lines represent nonbonded contacts (between 3.3 and 3.5 Å) between protein side chains and mandelate in the hydride transfer configuration. The green dashed lines represent interactions between the C2 hydrogen and the flavin N5 and/or His247 $N^{\epsilon 2}$ atom for the two models. This figure was prepared using Turbo-Frodo (*63*).

substrate is than that of LCHAO, whose physiological substrate is unknown, and of the other two enzymes.

The chemical mechanism for substrate oxidation in this enzyme family has long been considered to involve the initial formation of a carbanion, with the catalytic histidine abstracting the substrate C2 hydrogen as a proton (*45*−*48*). It has, however, been proposed more recently that it could involve a hydride transfer to the flavin, with the catalytic histidine abstracting the hydroxyl proton (*41*, *49*, *50*). Modeling L-lactate into the active site of FCB2 suggested that two binding modes were possible; one was compatible with a carbanion mechanism and the other one with a hydride transfer reaction (*43*). In both models, the carboxylate is bound as that of pyruvate in the WT FCB2 crystal structure. For the carbanion mechanism, the C2 hydroxyl forms a hydrogen bond with Tyr254 (position 129 of LCHAO) and the α-hydrogen points toward His373 (position 247 of LCHAO), whereas for the hydride transfer mechanism, the α-hydrogen points toward N5 of the flavin and the C2 hydroxyl oxygen forms a hydrogen bond with $N^{\epsilon 2}$ of His373.

Modeling studies, undertaken with FCB2 in an effort to understand why mandelate is so slow as a substrate (k_{cat} = 0.012 s^{-1} vs 250 s^{-1} with lactate), have been described (*44*). When the lactate methyl group, which is in van der Waals contact with the Ala198 (position 78 of LCHAO) methyl group, was replaced with the mandelate phenyl ring, the latter interfered with Ala198 and Leu230, whatever its orientation. After a clockwise rotation around the mandelate C1−C2 bond, an orientation could be found in which the unhindered phenyl ring is further away from the flavin and interfering side chains, and the substrate seems to be poised for a hydride transfer to N5 of flavin (*44*). This second mandelate binding mode corresponds to the lactate binding mode for the putative hydride transfer mechanism.

We have attempted to model mandelate into the active site of LCHAO (Figure 7). Initially, the carboxylate and C2 atoms of mandelate were superimposed onto those of pyruvate in the homologous FCB2 molecule after superposition of FCB2 onto the LCHAO model. Rotations about the C1−C2 bond and the C2−CG bond of the L-mandelate model were then made to configure the hydride transfer model, with the C2 hydrogen atom pointing toward the N5 atom of the flavin, with minimal overlap between atoms. The carbanion model was then obtained by rotating mandelate about the C1−C2 bond so that the C2 hydrogen atom moved toward the $N^{\epsilon 2}$ atom of His247 for proton abstraction. We find in this case also that a satisfactory model for hydride transfer is possible but not for the carbanion mechanism.

In view of the modeling studies, one could be tempted to assume a hydride transfer mechanism for all substrates in the family. This hypothesis, however, does not provide an explanation for the large differences in efficiency with mandelate among the four enzymes. It does not provide an explanation either for the differences in efficiency between mandelate and glycolate for GOX or lactate for FCB2. Could one then suppose, for these two enzymes, a different mechanism for mandelate and the physiological substrate? This hypothesis cannot be ruled out, but then the hydride transfer would be a highly disfavored reaction. The final possibility is a common carbanion mechanism for all substrates. As proposed before for FCB2, mandelate would be mostly bound as for a hydride transfer reaction, and its oxidation would occur only rarely when by chance a favorable constellation of side chain movements would enable the compound to bind in a mode better suited but still far from optimal for carbanion formation, with a high energy barrier (*44*). Apparently, such a barrier would be lower in the case of MDH since the side chains near the active site appear to be less constraining. Preliminary modeling of mandelate into the active site of MDH−GOX2 supports this conclusion (unpublished results).

The hypothesis of a unique mechanism for all substrates was apparently supported by site-directed mutagenesis, which relieved the steric hindrance to the carbanion binding mode in an A198G/L230A double mutant FCB2, with a 400-fold increased rate with mandelate, but with a low rate and a decreased efficiency with lactate (*51*, *52*). Conversely, the inverse Gly81Ala mutation in MDH decreases the enzyme activity with mandelate ~20-fold (*53*), in agreement with the idea that the methyl group of Ala interferes with the optimal orientation for a carbanion mechanism, whereas it does not seem to interfere with the binding mode postulated for a hydride transfer. No mutation at the corresponding Ala78 of LCHAO is yet available.

The crystal structure of the phenylglyoxylate-bound L230A mutant FCB2 was published recently (*41*); at the resolution

that was obtained, it is identical to that of the WT enzyme, except for the missing leucine side chain replaced with the alanine methyl group. For this mutant enzyme, the rate increase with respect to the WT enzyme is 5.5. From the orientation of the phenylglyoxylate aromatic group, combined with a model of bound mandelate, the authors conclude that the normal mandelate binding mode is incompatible with a carbanion reaction, and therefore that the reaction must proceed by hydride transfer. While we agree with the first part of this interpretation, in our opinion it does not clarify why the mutations improve so significantly the efficiency of mandelate, as just discussed.

A conclusion to be drawn from these two opposing views is that structural data in this case, even combined with modeling, do not provide a firm mechanistic result. One of the reasons may be that interpretations of crystal structures in terms of function do not take protein dynamics into account. This may be a particularly important factor in this enzyme family, and for LCHAO in particular. Examination of various liganded forms of GOX reveals a significant flexibility of a number of active site residues (*6*, *18*, *39*, *40*). LCHAO is a GOX isozyme and is also an oxidase. Although its crystal structure is very similar to that of FCB2 and MDH, which are both electron transferases, it could be endowed with the same mobility at and around the active site as GOX, as discussed in the next section. This may explain why it is more active than FCB2 with mandelate, although still a reasonably slow catalyst.

It thus appears that structures by themselves do not solve the mechanistic issue. Nevertheless, several results obtained in solution with the WT enzymes appear to rule out a hydride transfer mechanism. One of these is the demonstration that the FCB2 enzyme group that removes the substrate α-hydrogen has a pK_a of 9 in the reduced enzyme, a figure which can be ascribed to only the active site histidine and not to N5 of flavin (*47*). Another one, to quote but a few, is the observation of a low-temperature intermediate in the reaction of MDH with its substrate, which was identified as a charge-transfer complex between oxidized flavin and a carbanion/enediolate after loss of the substrate α-hydrogen (*48*). The primary deuterium isotope effect determined for its formation with 2-[^{2}H]mandelate appears to rule out the hypothesis that it could be an oxidized flavin−alkoxide complex, as interpreted by others (*50*).

Alternative Modes of Flavin Binding: Implications for the Oxidative Half-Reaction. A comparison of the structures of the flavin binding domains of FCB2 and GOX showed that, although their tertiary structures were very similar, there was a difference in the orientations of the flavin rings and how they interacted with the protein environment (*11*). These differences included the absence in GOX of a hydrogen bond from a backbone amide group of strand β1 to N5 of flavin and the presence of a water molecule bridging O4 and Ser106. In FCB2, the equivalent serine side chain, Ser228, binds directly to O4 and the water binding pocket is absent. It was hypothesized that in GOX the water binding site adjacent to O4 of flavin could serve as a binding site for dioxygen prior to attack by the reduced flavin in the oxidative half-reaction and lead to a covalent hydroperoxy intermediate. The absence of this putative dioxygen-binding pocket in FCB2 thus explained the weak reactivity of dioxygen with FCB2 compared to GOX. The structure of MDH−GOX2, which also reacts with dioxygen very slowly (*54*), also lacks the putative dioxygen-binding pocket, being very similar to FCB2 with respect to the orientation and interactions of the flavin ring.

The structure of LCHAO throws this hypothesis into question, since the flavin environment and mode of binding to the apoprotein are very similar to those in FCB2 and MDH−GOX2 despite the fact that LCHAO is an oxidase. However, the structures of two enzyme−inhibitor complexes of GOX, one with 4-carboxy-5-(1-pentyl)hexylsulfanyl-1,2,3-triazole (TACA) and the other with 3-decyl-2,5-dioxo-4-hydroxy-3-pyrroline (TKP) (*18*), reveal that in these two complexes the flavin ring has reoriented to a position nearly identical to that in LCHAO, FCB2, and MDH−GOX2. These GOX structures indicate that the isoalloxazine ring displays considerable flexibility of movement within this molecule. Flexibility of the flavin ring has also been observed in another flavoenzyme (*55*). LCHAO and the two GOX structures having the same flavin orientation as LCHAO also have a ligand bound at the active site, whereas uncomplexed GOX [the WT and a Tyr24Phe mutant of GOX (*39*)] has the altered flavin orientation. GOX follows a ping-pong mechanism where oxidized product dissociation occurs prior to enzyme reoxidation (*56*, *57*); the oxidative step could then involve reorientation of the flavin and opening of the dioxygen-binding pocket to allow the C4 atom of the flavin to react. The presence of the ligand would then stabilize the enzyme form lacking the water/dioxygen pocket; ligand dissociation would destabilize it. The same hypothesis can be formulated for LCHAO. FCB2 and MDH, which both react slowly with dioxygen, would presumably undergo flavin reorientation much less readily or not at all on product dissociation.

An intriguing point remains unexplained by the structure, that of the flavin N3 low pK_a in LCHAO (7.9 pH units) relative to free flavin [10 pH units (*58*)], a property shared with GOX (*15*, *56*, *57*). For WT GOX, the phenomenon was ascribed to the hydrogen bond observed in the crystal structure of the unliganded enzyme between O4 of FMN and the OH group of Tyr129, because the Tyr129Phe mutant GOX had a normalized pK_a (*40*). In the unliganded LCHAO, the same situation might occur, since binding of some ligands induced a normalization of the pK_a of LCHAO at N3. This could correspond to displacement of a putative hydrogen bond from Tyr129 to O4 of FMN in the free active site if LCHAO behaves like GOX. The LCHAO isozyme β2, with the basic three-residue insertion (VRK), has a pK_a even lower than that of isozyme β1 by 0.4 pH unit (*15*). This insertion is located between positions 188 and 189 of the β1 sequence, immediately after the loop 4 segment of residues 181−188, 13 Å from the flavin N3 atom. Since the segment that follows is not visible in the LCHAO structure, no hint of its interactions is given, and the effect of the three-residue insertion remains mysterious.

ACKNOWLEDGMENT

Use of the Advanced Photon Source was supported by the U.S. Department of Energy, Basic Energy Sciences, Office of Science, under Contract W-31-109-Eng-38. We also thank the staff at the Structural Biology Center for their assistance in the use of their equipment.

SUPPORTING INFORMATION AVAILABLE

Analysis of space group and subunit arrangement. This material is available free of charge via the Internet at http://pubs.acs.org.

REFERENCES

1. Lederer, F. (1991) in *Chemistry and biochemistry of the flavoenzymes* (Müller, F., Ed.) pp 153−242, CRC Press, Boca Raton, FL.
2. Ghisla, S., and Massey, V. (1991) in *Chemistry and biochemistry of the flavoenzymes* (Müller, F., Ed.) pp 243−289, CRC Press, Boca Raton, FL.
3. Maeda-Yorita, K., Aki, K., Sagai, H., Misaki, H., and Massey, V. (1995) L-Lactate oxidase and L-lactate monooxygenase: Mechanistic variations on a common structural theme, *Biochimie 77*, 631−642.
4. Lehoux, I. E., and Mitra, B. (1999) (*S*)-Mandelate dehydrogenase from *Pseudomonas putida*: Mechanistic studies with alternate substrates and pH and kinetic isotope effects, *Biochemistry 38*, 5836−5848.
5. Lê, K. H. D., and Lederer, F. (1991) Amino acid sequence of long chain α-hydroxy acid oxidase from rat kidney, a member of the family of fmn-dependent α-hydroxy acid-oxidizing enzymes, *J. Biol. Chem. 266*, 20877−20881.
6. Lindqvist, Y. (1989) Refined structure of spinach glycolate oxidase at 2 Å resolution, *J. Mol. Biol. 209*, 151−166.
7. Lindqvist, Y., and Brändén, C. I. (1980) Structure of glycolate oxidase from spinach at a resolution of 5.5 Å, *J. Mol. Biol. 143*, 201−211.
8. Xia, Z.-x., and Mathews, F. S. (1990) Molecular structure of flavocytochrome b_2 at 2.4 Å resolution, *J. Mol. Biol. 212*, 837−863.
9. Sukumar, N., Xu, Y., Gatti, D. L., Mitra, B., and Mathews, F. S. (2001) Structure of an active soluble mutant of the membrane-associated (*S*)-mandelate dehydrogenase, *Biochemistry 40*, 9870−9878.
10. Sukumar, N., Dewanti, A. R., Mitra, B., and Mathews, F. S. (2004) High-resolution structures of an oxidized and reduced flavoprotein: The water switch in a soluble form of (*S*)-mandelate dehydrogenase, *J. Biol. Chem. 279*, 3749−3757.
11. Lindqvist, Y., Brändén, C. I., Mathews, F. S., and Lederer, F. (1991) Spinach glycolate oxidase and yeast flavocytochrome b_2 are structurally homologous and evolutionarily related enzymes with distinctly different function and flavin mononucleotide binding, *J. Biol. Chem. 266*, 3198−3207.
12. Blanchard, M., Green, D. E., Nocito, V., and Ratner, S. (1944) L-Amino acid oxidase of animal tissue, *J. Biol. Chem. 155*, 421−440.
13. Blanchard, M., Green, D. E., Nocito-Carroll, V., and Ratner, S. (1946) L-Hydroxy acid oxidase, *J. Biol. Chem. 163*, 137−144.
14. Belmouden, A., Lê, K. H. D., Lederer, F., and Garchon, H.-J. (1993) Molecular cloning and nucleotide sequence of cDNA encoding rat kidney long-chain l-2-hydroxy acid oxidase. Expression of the catalytically active recombinant protein as a chimaera, *Eur. J. Biochem. 214*, 17−25.
15. Belmouden, A., and Lederer, F. (1996) The role of a β barrel loop 4 extension in modulating the physical and functional properties of long-chain 2-hydroxy-acid oxidase isozymes, *Eur. J. Biochem. 238*, 790−798.
16. Tegoni, M., Begotti, S., and Cambillau, C. (1995) X-ray structure of two complexes of the Y143F flavocytochrome b_2 mutant crystallized in the presence of lactate or phenyllactate, *Biochemistry 34*, 9840−9850.
17. Cunane, L. M., Barton, J. D., Chen, Z. W., Welsh, F. E., Chapman, S. K., Reid, G. A., and Mathews, F. S. (2002) Crystallographic study of the recombinant flavin-binding domain of baker's yeast flavocytochrome b_2: Comparison with the intact wild-type enzyme, *Biochemistry 41*, 4264−4272.
18. Stenberg, K., and Lindqvist, Y. (1997) Three-dimensional structures of glycolate oxidase with bound active-site inhibitors, *Protein Sci. 6*, 1009−1015.
19. Brush, E. J., and Hamilton, G. A. (1981) Thiol-glyoxylate adducts as substrates for rat kidney L-α-hydroxy acid oxidase, *Biochem. Biophys. Res. Commun. 103*, 1194−1200.
20. Gunshore, S., Brush, E. J., and Hamilton, G. A. (1985) Equilibrium constants for the formation of glyoxylate thiohemiactals and kinetic constants for their oxidation by O_2 catalyzed by L-hydroxy acid oxidase, *Bioorg. Chem. 13*, 1−13.
21. Nakano, M. (1964) Comparison of the enzyme oxidizing thyroid hormone with L-amino acid oxidase, *Biochim. Biophys. Acta 92*, 472−481.
22. Stevens, J. L., Robbins, J. D., and Byrd, R. A. (1986) A purified cysteine conjugate β-lyase from rat kidney cytosol. Requirement for an α-keto acid or an amino acid oxidase for activity and identity with soluble glutamine transaminase k, *J. Biol. Chem. 261*, 15529−15537.
23. Stevens, J. L., Hatzinger, P. B., and Hayden, P. J. (1989) Quantitation of multiple pathways for the metabolism of nephrotoxic cysteine conjugates using selective inhibitors of L-α-hydroxy acid oxidase (L-amino acid oxidase) and cysteine conjugate $\beta\delta$-lyase, *Drug Metab. Dispos. 17*, 297−303.
24. Ozasa, H., Horikawa, S., and Ota, K. (1994) Methylguanidine synthase from rat kidney is identical to long-chain L-2-hydroxy acid oxidase, *Nephron 68*, 279.
25. Yokozawa, T., Fujitsuka, N., Oura, H., Akao, T., Kobashi, K., Ienaga, K., Nakamura, K., and Hattori, M. (1993) Purification of methylguanidine synthase from the rat kidney, *Nephron 63*, 452−457.
26. Jones, J. M., Morrell, J. C., and Gould, S. J. (2000) Identification and characterization of haox1, haox2, and haox3, three human peroxisomal 2-hydroxy acid oxidases, *J. Biol. Chem. 275*, 12590−12597.
27. Jones, J. M., Morrell, J. C., and Gould, S. J. (2004) Identification and characterization of haox1, haox2, and haox3, three human peroxisomal 2-hydroxy acid oxidases, *J. Biol. Chem. 275*, 35122.
28. Cunane, L. M., Barton, J. D., Chen, Z.-w., Mathews, F. S., Belmouden, A., Lê, K. H. D., Welsh, F. E., Chapman, S. K., and Reid, G. A. (1999) in *Flavins and Flavoproteins 1999* (Ghisla, S., Kroneck, P., Macheroux, P., and Sund, H., Eds.) pp 459−462, Weber, Konstanz, Germany.
29. McPherson, A. (1999) *Crystallization of biological macromolecules*, Cold Spring Harbor Laboratory Press, Plainview, NY.
30. Otwinowski, Z., and Minor, W. (1997) Processing of X-ray diffraction data collected by oscillation methods, *Methods Enzymol. 276*, 307−326.
31. Navaza, J. (1994) Amore: An automated package for molecular replacement, *Acta Crystallogr. A50*, 157−163.
32. Lindqvist, Y., and Brändén, C. I. (1989) The active site of spinach glycolate oxidase, *J. Biol. Chem. 264*, 3624−3628.
33. Brünger, A. (1993) *X-plor (version 3.1): A system for X-ray crystallography and NMR*, Yale University Press, New Haven, CT.
34. Brünger, A. T., Adams, P. D., Clore, G. M., DeLano, W. L., Gros, P., Grosse-Kunstleve, R. W., Jiang, J. S., Kuszewski, J., Nilges, M., Pannu, N. S., Read, R. J., Rice, L. M., Simonson, T., and Warren, G. L. (1998) Crystallography & NMR system: A new software suite for macromolecular structure determination, *Acta Crystallogr. D54*, 905−921.
35. Gould, S. J., Krisans, S., Keller, G. A., and Subramani, S. (1990) Antibodies directed against the peroxisomal targeting signal of firefly luciferase recognize multiple mammalian peroxisomal proteins, *J. Cell Biol. 110*, 27−34.
36. Laskowski, R., Thornton, J., Moss, D., and MacArthur, M. (1993) Procheck: A program to check the stereochemical quality of protein structures, *J. Appl. Crystallogr. 26*, 283−291.
37. Ramakrishnan, C., and Ramachandran, G. N. (1965) Stereochemical criteria for polypeptide and protein chain conformations. II. Allowed conformations for a pair of peptide units, *Biophys. J. 5*, 909−933.
38. Phillips, D. R., Duley, J. A., Fennell, D. J., and Holmes, R. S. (1976) The self-association of L-α-hydroxy acid oxidase, *Biochim. Biophys. Acta 427*, 679−687.
39. Stenberg, K., Clausen, T., Lindqvist, Y., and Macheroux, P. (1995) Involvement of Tyr24 and Trp108 in substrate binding and substrate specificity of glycolate oxidase, *Eur. J. Biochem. 228*, 408−416.
40. Macheroux, P., Kieweg, V., Massey, V., Soderlind, E., Stenberg, K., and Lindqvist, Y. (1993) Role of tyrosine 129 in the active site of spinach glycolate oxidase, *Eur. J. Biochem. 213*, 1047−1054.
41. Mowat, C. G., Wehenkel, A., Green, A. J., Walkinshaw, M. D., Reid, G. A., and Chapman, S. K. (2004) Altered substrate specificity in flavocytochrome b_2: Structural insights into the mechanism of L-lactate dehydrogenation, *Biochemistry 43*, 9519−9526.

42. Fraaije, M. W., and Mattevi, A. (2000) Flavoenzymes: Diverse catalysts with recurrent features, *Trends Biochem. Sci. 25*, 126−132.
43. Lederer, F. (1991) in *Flavins and flavoproteins 1990* (Curti, B., Ronchi, S., and Zanetti, G., Eds.) pp 773−782, Walter de Gruyter, Berlin.
44. Gondry, M., Dubois, J., Terrier, M., and Lederer, F. (2001) The catalytic role of tyrosine 254 in flavocytochrome b_2 (L-lactate dehydrogenase from baker's yeast): Comparison between the Y254F and Y254L mutant proteins, *Eur. J. Biochem. 268*, 4918−4927.
45. Walsh, C., Lockridge, O., Massey, V., and Abeles, R. (1973) Studies on the mechanism of action of the flavoenzyme lactate oxidase. Oxidation and elimination with β-chlorolactate, *J. Biol. Chem. 248*, 7049−7054.
46. Lederer, F. (1997) in *Flavins and flavoproteins 1996* (Stevenson, K., Massey, V., and Williams, C. H., Jr., Eds.) pp 545−553, University of Calgary Press, Calgary, AB.
47. Rao, K. S., and Lederer, F. (1998) About the pK_a of the active-site histidine in flavocytochrome b_2 (yeast L-lactate dehydrogenase), *Protein Sci. 7*, 1531−1537.
48. Dewanti, A. R., and Mitra, B. (2003) A transient intermediate in the reaction catalyzed by (s)-mandelate dehydrogenase from *Pseudomonas putida*, *Biochemistry 42*, 12893−12901.
49. Mattevi, A., Vanoni, M. A., Todone, F., Rizzi, M., Teplyakov, A., Coda, A., Bolognesi, M., and Curti, B. (1996) Crystal structure of D-amino acid oxidase: A case of active site mirror-image convergent evolution with flavocytochrome b_2, *Proc. Natl. Acad. Sci. U.S.A. 93*, 7496−7501.
50. Sobrado, P., and Fitzpatrick, P. F. (2003) Solvent and primary deuterium isotope effects show that lactate CH and OH bond cleavages are concerted in Y254F flavocytochrome b_2, consistent with a hydride transfer mechanism, *Biochemistry 42*, 15208−15214.
51. Sinclair, R., Reid, G. A., and Chapman, S. K. (1998) Re-design of *Saccharomyces cerevisiae* flavocytochrome b_2: Introduction of L-mandelate dehydrogenase activity, *Biochem. J. 333*, 117−120.
52. Daff, S., Manson, F. D., Reid, G. A., and Chapman, S. K. (1994) Strategic manipulation of the substrate specificity of *Saccharomyces cerevisiae* flavocytochrome b_2, *Biochem. J. 301*, 829−834.
53. Dewanti, A. R., Xu, Y., and Mitra, B. (2004) Role of glycine 81 in (S)-mandelate dehydrogenase from *Pseudomonas putida* in substrate specificity and oxidase activity, *Biochemistry 43*, 10692−10700.
54. Xu, Y., and Mitra, B. (1999) in *Flavins and Flavoproteins 1999* (Ghisla, S., Kroneck, P., Macheroux, P., and Sund, H., Eds.) pp 487−490, Agency for Scientific Publications, Berlin.
55. Gatti, D. L., Palfey, B. A., Lah, M. S., Entsch, B., Massey, V., Ballou, D. P., and Ludwig, M. L. (1994) The mobile flavin of 4-OH benzoate hydroxylase, *Science 266*, 110−114.
56. Schuman, M., and Massey, V. (1971) Purification and characterization of glycolic acid oxidase from pig liver, *Biochim. Biophys. Acta 227*, 500−520.
57. Macheroux, P., Massey, V., Thiele, D. J., and Volokita, M. (1991) Expression of spinach glycolate oxidase in *Saccharomyces cerevisiae*: Purification and characterization, *Biochemistry 30*, 4612−4619.
58. Muller, F. (1991) in *Chemistry and biochemistry of flavoenzymes* (Muller, F., Ed.) pp 1−71, CRC Press, Boca Raton, FL.
59. Filipe, A., Belmouden, A., Lacombe, J.-M., and Lederer, F. (1997) in *Flavins and flavoproteins 1996* (Stevenson, K., Massey, V., and Williams, C. H., Jr., Eds.) pp 559−562, University of Calgary Press, Calgary, AB.
60. Xu, Y., and Mitra, B. (1999) A highly active, soluble mutant of the membrane-associated (S)-mandelate dehydrogenase from *Pseudomonas putida*, *Biochemistry 38*, 12367−12376.
61. Kraulis, P. J. (1991) Molscript: A program to produce both detailed and schematic plots of protein structures, *J. Appl. Crystallogr. 24*, 946−950.
62. Merritt, E. A., and Bacon, D. J. (1997) Raster 3d: Photorealistic molecular graphics, *Methods Enzymol. 277*, 505−524.
63. Roussel, A., and Cambillau, C. (1989) in *Silicon graphics geometry partners directory*, pp 77−78, Silicon Graphics, Mountain View, CA.

BI048616E